Supplementary Materials

Efficient photocatalytic hydrogen production under visible-light irradiation with 2D Molybdenum nitride cocatalyst

Xiangjiu Guan[1,*,#], Yi Yuan[1,#], Li Tian[1,#], Zhenxiong Huang[2,*], Xiaoyuan Ye[1], Tuo Zhang[1], Bin Zhu[1], Zhifu Zhou[1]

[1]International Research Center for Renewable Energy, State Key Laboratory of Multiphase Flow in Power Engineering, Xi'an Jiaotong University, Xi'an 710049, Shaanxi, China.
[2]Institute of Energy Research, Jiangxi Academy of Sciences, Nanchang 330096, Jiangxi, China.
[#]Authors contributed equally.

Correspondence to: Prof. Xiangjiu Guan, International Research Center for Renewable Energy, State Key Laboratory of Multiphase Flow in Power Engineering, Xi'an Jiaotong University, No. 28, Xianning West Road, Xi'an 710049, Shaanxi, China. E-mail: xj-guan@mail.xjtu.edu.cn; Dr. Zhenxiong Huang, Institute of Energy Research, Jiangxi Academy of Sciences, No. 7777 Changdong Avenue, Nanchang 330096, Jiangxi, China. E-mail: huangzhenxiong@jxas.ac.cn

ORCID: Xiangjiu Guan (0000-0003-1877-3282), Zhenxiong Huang (0000-0002-0748-4621)

CHARACTERIZATION

X-ray diffraction (XRD) patterns were recorded from a diffractometer (X'pert PRO MPD, PANalytical, Netherlands) using Ni-filtered Cu Kα irradiation with an operating condition of 40 kV and 40 mA and a rate of 2^o min^{-1} in the 2θ range from 10 to 80^o. XPS spectra were recorded on an X-ray photonic spectrometer (ESCALAB Xi+, Thermo Fisher, USA). UV-vis spectra were collected by UV-vis-near-IR spectrophotometer (Agilent Cary 5000) with $BaSO_4$ reference, with Kubelka-Munk (K-M) method adopted for estimation of bandgap energy. Scanning electron microscopy (SEM) images were observed by a field-emission scanning electron microscope (JSM-7800F, JEOL, Japan). High-resolution transmission electron microscopy (HRTEM) image was obtained from a transmission electron microscope (JEM-2100, JEOL, Japan) at an accelerating voltage of 200 kV. Elemental mapping images were obtained from OXFORDMAX-80 energy-dispersive X-ray detector equipped on transmission electron microscope (Tecnai G2 F30 S-Twin, FEI, Netherlands). The photoluminescence spectra (PL) analysis was conducted on a PTI QuantaMaster 40 steady-state fluorescence spectrophotometer at room temperature with a solid-state sample.

Electrochemical tests were conducted on the CHI760E electrochemical workstation (CH Instrument, China). For the linear sweep voltammetry (LSV) test, a three-electrode cell was used including the counter electrode (Pt slice), the reference electrode (Ag/AgCl), and the working electrode (photocatalysts on a glassy carbon electrode), and Na_2SO_4 aqueous solution (0.5 M, pH = 6.8) was used as the electrolyte. Electrochemical impedance spectroscopy (EIS) was obtained with an applied voltage (-0.6 V vs. Ag/AgCl) and the frequency range (100 kHz ~ 0.1 Hz). The transformation of potentials vs. Ag/AgCl and RHE was calculated as follows:

$$E_{RHE} = E_{Ag/AgCl} + 0.0591 \times pH + E^0_{Ag/AgCl} \quad (E^0_{Ag/AgCl} = 0.1976 \text{ V at } 25\ °C) \qquad (S1)$$

DFT CALCULATION

The work function and charge transfer between CdS and $MoN_{1.2}$ were evaluated by first principle simulation achieved by VASP codes under the level of generalized gradient approximation (GGA) by Perdew-Burke-Ernzerhof functional. The original crystal structures were exported from Material Project Database. For the $MoN_{1.2}$, the fraction occupancy of Mo site was represented by virtual crystal approximation (VCA), and both the crystal cell was geometric optimized by conjugate gradient method. The self-consistent field calculation converged under the energy criterion of 10-7eV with the gamma-center k mesh of 0.03 2π/Å density. The work function was calculated by the difference between average vacuum energy level and Fermi level in the slab model of CdS and $MoN_{1.2}$. In order to study the interface charge transfer, the electron density difference analysis was deployed on the heterojunction slab model along (001) crystallographic direction, which constructed based on the integer ratio of lattice parameters.

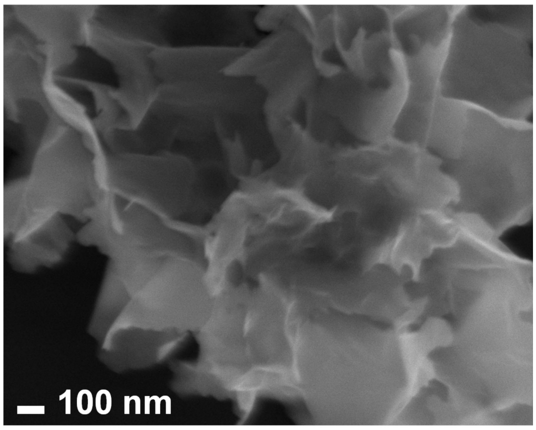

Supplementary Figure 1. SEM image of MN.

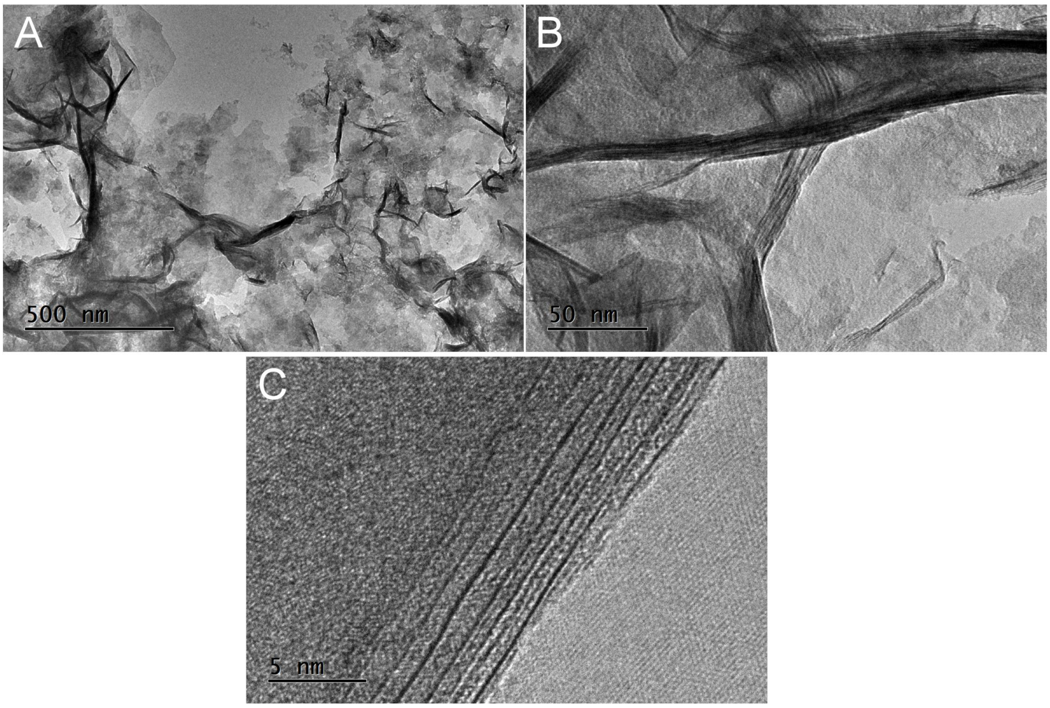

Supplementary Figure 2. (A) TEM and (B, C) HRTEM images of MN.

Supplementary Figure 2A shows the nanosheet morphology of as-prepared MN, as also indicated from Supplementary Figure 1. Moreover, clear layered structure of MN has also been demonstrated from HRTEM images in Supplementary Figure 2B and C.

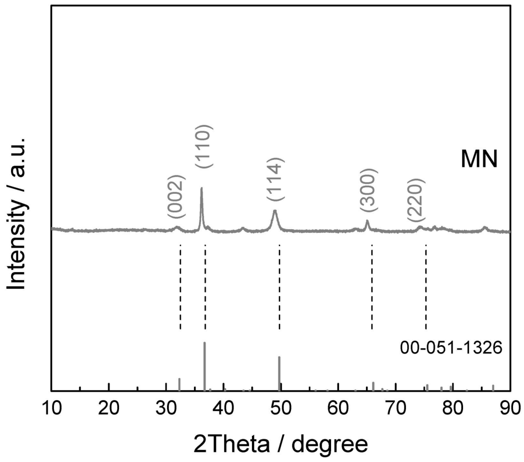

Supplementary Figure 3. XRD pattern of MN compared with standard Mo_5N_6.

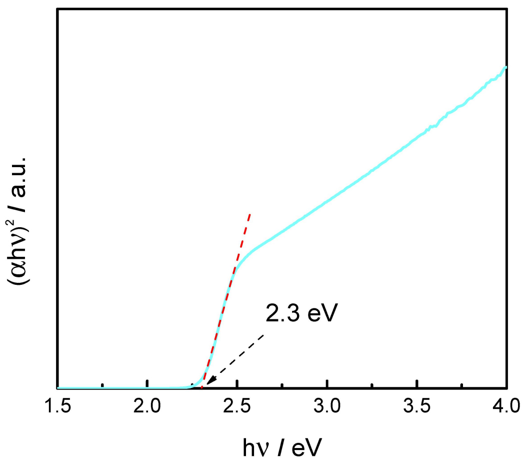

Supplementary Figure 4. Tauc plot via Kubelka-Munk method for estimating the bandgap of CdS.

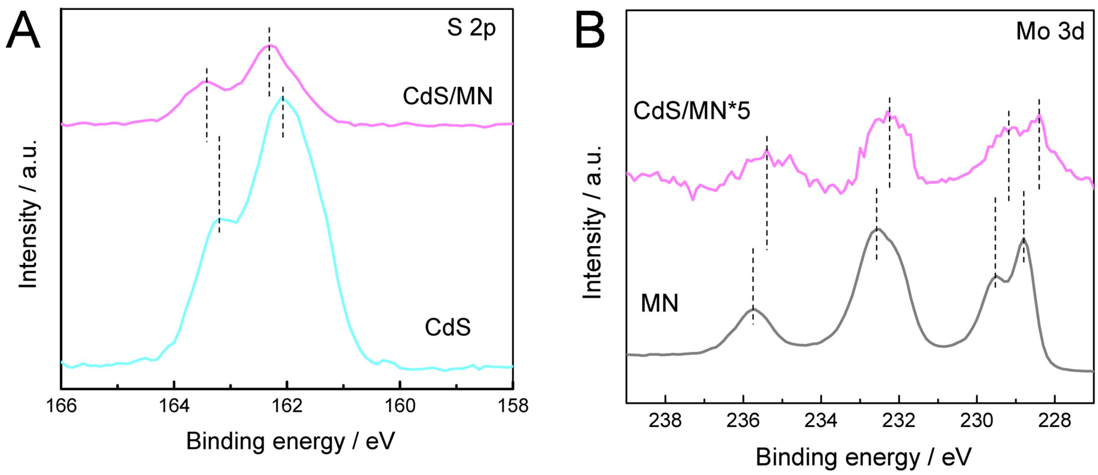

Supplementary Figure 5. XPS spectra. (A) S 2p orbitals of CdS and CdS/MN; (B) Mo 3d orbitals of MN and CdS/MN.

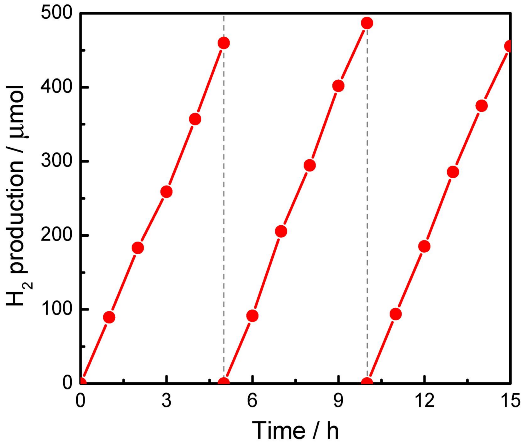

Supplementary Figure 6. Stability test of CdS/MN for photocatalytic hydrogen production under AM1.5G (4 mg photocatalyst was used)

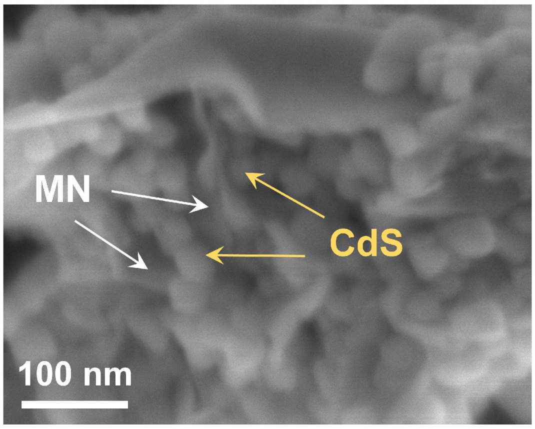

Supplementary Figure 7. SEM image of CdS/MN after photocatalytic reaction.

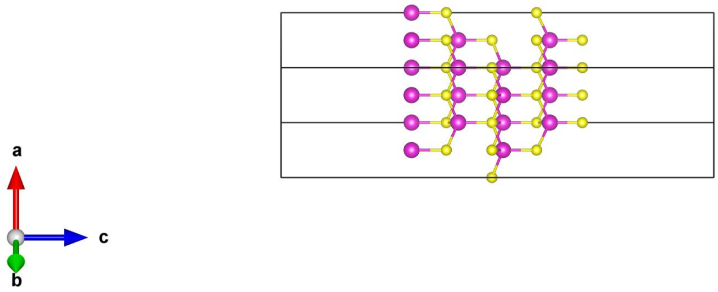

Supplementary Figure 8. Slab model of CdS for DFT calculation.

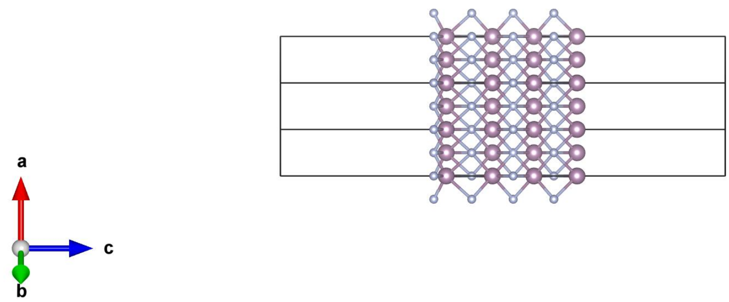

Supplementary Figure 9. Slab model of $MoN_{1.2}$ for DFT calculation.

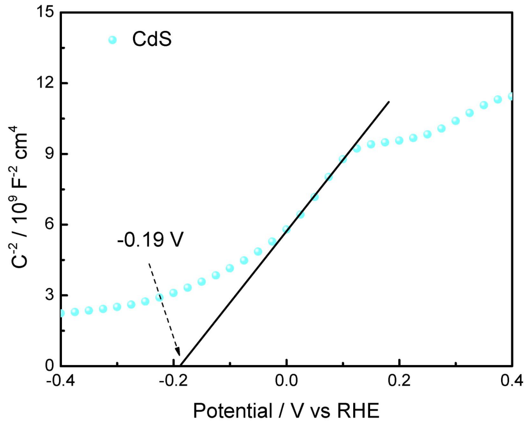

Supplementary Figure 10. Mott-Schottky curve of CdS.

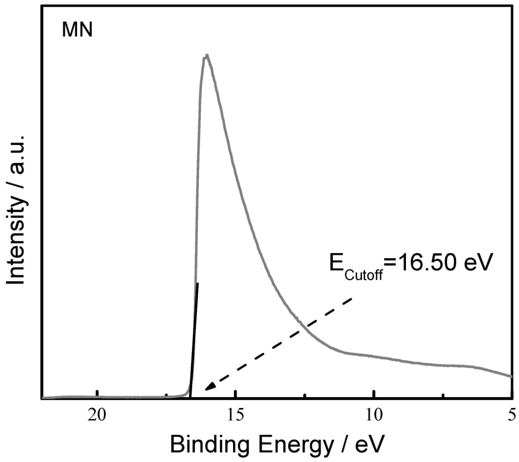

Supplementary Figure 11. Cutoff region of UPS spectrum of MN.

The cutoff edge of band energy in UPS spectrum is 16.50 eV, indicating a work function of 4.72 eV (Φ=21.22-E_{cutoff}), hence the corresponding fermi level of MN is ~0.28 V vs NHE.

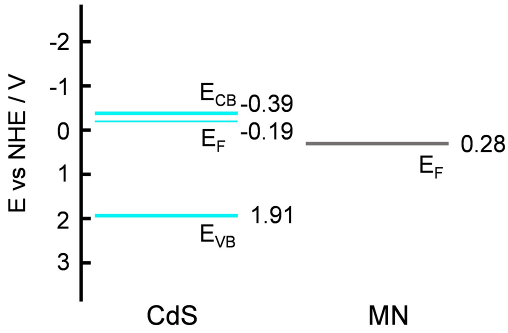

Supplementary Figure 12. Band diagram of CdS and MN.

Mott-Schottky test in Supplementary Figure 10 indicates a flatband potential of CdS at ~-0.19 V, which is near to the fermi level (E_F). As for n-type semiconductors like CdS, the conduction band minimum position (E_{CB}) is slightly negative than flatband potential by ~0.2 V, hence is estimated at ~-0.39 V. Given that band gap of CdS is 2.3 eV (Supplementary Figure 4), the valence band maximum position (E_{VB}) could be obtained as 1.91 V. Besides, E_F of MN could be obtained from the cutoff region of UPS spectrum, as depicted in Supplementary Figure 12.

Supplementary Table 1. The calculated structural parameters of CdS, MN and CdS/MN

Sample	Component	Lattice constant						Crystallite size (nm)
		a (Å)	b (Å)	c (Å)	α	β	γ	
CdS	CdS	4.1458	4.1458	6.7432	90	90	120	41.2
MN	MN	5.73912	5.73912	5.62951	90	90	120	18.1
CdS/MN	CdS	4.13199	4.13199	6.72837	90	90	120	40.9

The structural parameters were calculated based on the XRD results in Figure 2A.

The calculated lattice constants of CdS are close to those of hexagonal CdS in the database (00-001-0780), with the crystallite size calculated as 41.2 nm, which is close to that observed in SEM images. Lattice constants and crystallite size of CdS in CdS/MN composite exhibit very slight changes compared with pare CdS, indicating that the fabrication of composite has scarcely influence the intrinsic properties of CdS.

The calculated lattice constants of MN are significantly different from those of hexagonal Mo_5N_6 in the database (00-001-0780). As discussed in the XRD analysis, although the as-synthesized molybdenum nitride exhibits similar XRD pattern with standard Mo_5N_6, while the diffraction peaks are significantly shifted towards low angles. When combined with the calculated lattice constants here, it could be ascribed to the characteristics of 2D layered structure. The as-synthesized molybdenum nitride, following by the previously reported procedure in ***Chem 2020, 6, 2382–2394*** (https://doi.org/10.1016/j.chempr.2020.06.037), is indeed 2D layered $MoN_{1.2}$ instead of Mo_5N_6.

Supplementary Table 2. Fitting parameters for TRPL spectra of CdS and CdS/MN

Sample	**A_1**	**τ_1 (ns)**	**A_2**	**τ_2 (ns)**	**$\tau_{average}$ (ns)**
CdS	0.56	0.44	0.25	4.12	3.40
CdS/MN	0.54	0.65	0.19	5.88	4.63

To extract the PL lifetimes, we used a biexponential function [$F(t)=y_0+\sum_i \alpha_i e^{-t/\tau_i}$, i= 1, 2] to fit the PL decay data, where a denotes the amplitude fractions ($\sum_i \alpha_i = 1$) and τ_i is the carrier lifetime. We used a two-component equation describing thesurface and possible defect-mediated (fast) and bulk (slow) radiative charge-carrier recombination, respectively.

The average lifetime $\tau_{average}$ was calculated by the equation:

$$\tau_{average} = {(\sum_i \alpha_i \tau_i^2)}/{(\sum_i \alpha_i \tau_i)} \quad (i = 1, 2) \qquad \text{(S2)}$$

Supplementary Table 3. Fitted EIS parameters of CdS and CdS/MN (with corresponding circuit displayed below)

Sample	R_S	R_{CT}
CdS	51.17	6610
CdS/MN	51.08	351.8

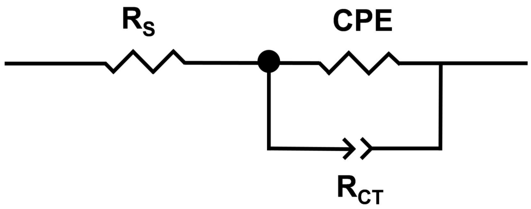

Supplementary Table 4. The specific parameters for quantum efficiency test of CdS/MN

DT (nm)	Intensity (W/m^2)	H_2 production (μmol/h)	AQY (%)
400	30.43	79.56	61.60
450	33.60	100.30	62.50
500	38.01	103.89	51.51
550	51.23	6.60	2.20
600	52.33	/	/
700	41.52	/	/

The spot area is 7.06 cm^2.

Supplementary Table 5. Comparison of CdS photocatalysts for H_2 production with earth-abundant cocatalysts

Catalysts	Sacrificial Reagent	Light Source	H_2 yields ($mmol\cdot h^{-1}\cdot g^{-1}$)	AQY	Ref.
CdS/MN	20% Lactic acid	λ ≥420 nm	58.4	62.5% (450 nm)	This Work
1D CdS@MoS_2	10% Lactic acid	λ≥420 nm	24.655	28.5% (420 nm)	[1]
CoP/CdS	10% Lactic acid	λ≥400 nm	104.947	32.16% (420 nm)	[2]
CDs/CdS	10% Lactic acid	AM 1.5 G	6.7	19.3% (420 nm)	[3]
Co_3N/CdS	0.75 M Na_2S and 1.05 M Na_2SO_3	λ≥420 nm	137.33	14.9% (450 nm)	[4]
MoP/CdS	20% Lactic acid	λ≥400 nm	13.88	66.7% (420 nm)	[5]
2D-2D MoS_2/CdS	0.4 M Na_2S and 0.4 M Na_2SO_3	λ≥420 nm	26.32	46.65% (450 nm)	[6]
MoS_2/CdS	20% Lactic acid	λ≥400 nm	95.7	46.9% (420 nm)	[7]
TpTAP/CdS	10% Ascorbic acid	λ≥420 nm	47.6	25.23% (420 nm)	[8]
WS_2–CdS	20% Lactic acid	λ≥400 nm	61.1	28.9% (420nm)	[9]
MoS_2/CdS	0.25 M Na_2SO_3 and 0.35 M Na_2S	λ≥420 nm	19	51.2% (420 nm)	[10]

Supplementary Table 6. Comparison of CdS/MN composite photocatalyst for H_2 production with CdS composited with 2D metal oxides

Catalysts	Sacrificial reagent	Light source	H_2 yields ($mmol \cdot h^{-1} \cdot g^{-1}$)	AQY	Ref.
CdS/MN	20% Lactic acid	λ≥420 nm	58.4	62.5% (450 nm)	This Work
CdS/α-Fe_2O_3	0.25 M Na_2S and 0.25 M Na_2SO_3	λ≥420 nm	1.806	13.7% (420 nm)	[11]
NiO/CdS	0.35 M Na_2S and 0.25 M Na_2SO_3	λ≥420 nm	15.6	17.1% (475 nm)	[12]
CdS/TiO_2(B)	0.1 M Na_2S and 0.1 M Na_2SO_3	λ≥420 nm	1.776	3.97% (420 nm)	[13]
CdS/WO_3	25% Ascorbic acid	λ≥420 nm	99.2	49.42% (600 nm)	[14]
CdS/MoO_{3-x}	10% Lactic acid	350 W Xenon lamp (full spectru,)	7.44	14.3% (450 nm)	[15]

Supplementary Table 7. Calculated results for work functions of CdS and CdS/MN

Sample	Vacuum level (eV)	Fermi level (eV)	Work function (eV)
CdS	3.58	-2.83	6.41
MN	7.15	0.24	6.91

REFERENCES

1. Han B, Liu S, Zhang N, Xu Y, Tang Z. One-dimensional CdS@MoS_2 core-shell nanowires for boosted photocatalytic hydrogen evolution under visible light. *Appl Catal B* 2017; 202: 298-304. DOI: 10.1016/j.apcatb.2016.09.023
2. Sun Q, Yu Z, Jiang R, et al. CoP QD anchored carbon skeleton modified CdS nanorods as a co-catalyst for photocatalytic hydrogen production. *Nanoscale* 2020; 12(37): 19203-19212. DOI: 10.1039/D0NR05268J
3. Zhu C, Liu C, Fu Y, et al. Construction of CDs/CdS photocatalysts for stable and efficient hydrogen production in water and seawater. *Appl Catal B* 2019; 242: 178-185. DOI: 10.1016/j.apcatb.2018.09.096
4. Chen H, Jiang D, Sun Z, Irfan RM, Zhang L, Du P. Cobalt nitride as an efficient cocatalyst on CdS nanorods for enhanced photocatalytic hydrogen production in water. *Catal Sci Techno* 2017;7(7): 1515-1522. DOI: 10.1039/C7CY00046D
5. Yang F, Liu D, Li Y, Ning S, Cheng L, Ye J. Solid-state synthesis of ultra-small freestanding amorphous MoP quantum dots for highly efficient photocatalytic H_2 production. *Chem Eng J* 2021; 406: 126838. DOI: 10.1016/j.cej.2020.126838
6. Yuan Y J, Li Z, Wu S, et al. Role of two-dimensional nanointerfaces in enhancing the photocatalytic performance of 2D-2D MoS_2/CdS photocatalysts for H_2 production. *Chem Eng J* 2018; 350: 335-343. DOI: 10.1016/j.cej.2018.05.172
7. He J, Chen L, Wang F, et al. CdS nanowires decorated with ultrathin MoS_2 nanosheets as an efficient photocatalyst for hydrogen evolution. *ChemSusChem* 2016; 9(6): 624-630. DOI: 10.1002/cssc.201501544
8. Gao R, Bai J, Shen R, et al. 2D/2D covalent organic framework/CdS Z-scheme heterojunction for enhanced photocatalytic H_2 evolution: Insights into interfacial charge transfer mechanism. *J Mater Sci Techno* 2023; 137: 223-231. DOI: 10.1016/j.jmst.2022.09.001
9. He J, Chen L, Yi Z Q, Au CT, Yin S. CdS nanorods coupled with WS_2 nanosheets for enhanced photocatalytic hydrogen evolution activity. *Ind Eng Chem Res* 2016; 55(30): 8327-8333. DOI: 10.1021/acs.iecr.6b01511

10. Patriarchea C, Vamvasakis I, Koutsouroubi ED, Armatas GS. Enhancing interfacial charge transfer in mesoporous MoS_2/CdS nanojunction architectures for highly efficient visible-light photocatalytic water splitting. *Inorg Chem Front* 2022; 9(4): 625-636. DOI: 10.1021/acs.iecr.6b01511

11. Guo F, Sun H, Shi Y, Zhou F, Shi W. CdS nanoparticles decorated hexagonal Fe_2O_3 nanosheets with a Z-scheme photogenerated electron transfer path for improved visible-light photocatalytic hydrogen production. *Chin J Chem Eng* 2022; 43: 266-274. DOI: 10.1016/j.cjche.2021.03.055

12. Wang P, Huang X, Dong T, Ren Y, Hu J. 2D black NiO with oxygen vacancies/1D CdS nanocomposites for efficient visible-light-driven photocatalytic H_2 production. *Appl Surf Sci* 2022; 606: 154940. DOI: 10.1016/j.apsusc.2022.154940

13. Luo X, Ke Y, Yu L, Wang Y, Homewood KP, Chen X, Gao Y. Tandem CdS/TiO_2(B) nanosheet photocatalysts for enhanced H_2 evolution. *Appl Surf Sci* 2020; 515: 145970. DOI: 0.1016/j.apsusc.2020.145970

14. Bharagav U, Reddy NR, Koteswararao VN, Ravi P, Pratap K, Sathish M, Cheralathan K, Shankar M, Kumari M. Heterojunction of CdS nanocapsules–WO_3 nanosheets composite as a stable and efficient photocatalyst for hydrogen evolution. *Energy & Fuels* 2020; 34(11): 14598-14610. DOI: 10.1021/acs.energyfuels.0c00597

15. Peng J, Shen J, Yu X, Tang H, Liu Q. Construction of LSPR-enhanced 0D/2D CdS/MoO_{3-x} S-scheme heterojunctions for visible-light-driven photocatalytic H_2 evolution. *Chin J Catal* 2021,; 42(1): 87-96. DOI: 10.1016/S1872-2067(20)63595-1